Asian Journal of Chemistry; Vol. 38, No. 2 (2026), 522-530
ASIAN JOURNAL OF CHEMISTRY
https://doi.org/10.14233/ajchem.2026.35150

Design, X-Ray Diffraction and *in silico* Analysis of Schiff Base Targeting HIV Reverse Transcriptase and Bacterial DNA Gyrase

G.M. PRADEEPALAKSHMI[1], VALARMATHY GOVINDARAJ[1,*] and SUBRAMANIAN RAMASAMY[2]

[1]PG and Research Department of Chemistry, Seethalakshmi Ramaswami College (Affiliated to Bharathidasan University, Tiruchirappalli), Tiruchirappalli-620002, India
[2]Division of Chemistry, School of Sciences, Faculty of Engineering and Technology, SRM Institute of Science and Technology, Tiruchirappalli-621105, India

*Corresponding author: E-mail: valarchola@gmail.com

Received: 28 October 2025 *Accepted*: 16 January 2026 *Published online*: 31 January 2026 AJC-22271

A green, catalyst-free synthesis yielded a new Schiff base, (*E*)-2-(((4-chlorophenyl)imino)methyl)-6-methoxyphenol, as orange single crystals suitable for X-ray diffraction. The compound crystallised in an orthorhombic lattice (space group $P2_12_12_1$), with a robust framework stabilised by intramolecular O–H···N hydrogen bonding and extended C–H···O/Cl contacts. Molecular docking revealed strong affinities toward HIV-1 reverse transcriptase (-8.4 kcal/mol) and bacterial DNA gyrase B (-7.1 kcal/mol), dominated by π–π stacking and hydrophobic interactions. Remarkably, even at low concentrations (50 μg mL^{-1}), the Schiff base displayed significant antibacterial efficacy against *Staphylococcus aureus* (11.35 ± 0.21 mm) and *Escherichia coli* (13.35 ± 0.21 mm), with higher inhibition zones than gentamicin at elevated doses. Its high gastrointestinal absorption, blood-brain barrier permeability and low predicted toxicity further endorse its drug-likeness. The combination of crystal stability, low-dose antibacterial efficiency and favourable docking profile identifies this Schiff base as a structurally and pharmacologically valuable scaffold for multifunctional antimicrobial development.

Keywords: Schiff base, X-ray diffraction, Molecular docking, Drug-likeness, Antiviral, Antibacterial, Toxicity.

INTRODUCTION

The design of organic molecules that combine structural stability with favourable pharmacological properties remains an important challenge in medicinal chemistry [1-4]. Schiff bases are particularly attractive in this regard because they are easily synthesised through the condensation of primary amines with carbonyl compounds, a reaction that proceeds under mild conditions with water as the only byproduct [5-9]. This simplicity not only highlights their atom economy but also aligns with the principles of green chemistry, making Schiff base synthesis environmentally benign and sustainable [10]. Beyond their eco-friendly preparation, Schiff bases are well known for their broad spectrum of biological activities, including antimicrobial, anticancer, antioxidant and antiviral properties, which are often attributed to the presence of the azomethine (–C=N–) functional group that facilitates diverse interactions with biomolecular targets [11-13]. While a large number of Schiff bases have been reported, most studies remain confined either to synthetic and crystallographic aspects or to computational and biological evaluations [14]. An integrated approach that links molecular structure to pharmacological potential is less common but essential for developing reliable drug candidates [15]. Subtle changes in substituents on the aromatic ring can significantly alter both crystal packing arrangements and binding affinity toward biological receptors, thereby influencing pharmacokinetic performance [16,17].

To explore these relationships, a Schiff base derived from *o*-vanillin (2-hydroxy-3-methoxybenzaldehyde) and 4-chloroaniline was synthesised and obtained as a single crystal suitable for X-ray diffraction analysis. The compound was identified as (*E*)-2-(((4-chlorophenyl)imino)methyl)-6-methoxyphenol, hereafter referred to as the Schiff base. In this work, the structural features of the synthesised Schiff base were established by single-crystal X-ray diffraction (SCXRD), which provided unambiguous confirmation of molecular geometry and hydrogen bonding interactions. The biological potential of this Schiff base was further investigated using molecular docking against selected protein targets. For this purpose, HIV-1 reverse transcriptase (1EVE, 1W6R) and bacterial DNA gyrase (5DEX) were sele-

cted as representative antiviral and antibacterial targets due to their relevance in infectious disease pathways. Its pharmacokinetic properties were predicted using the SwissADME platform, while the toxicity profile was assessed through the ProTox-II server. By integrating crystallographic validation with *in silico* docking, ADMET profiling and toxicity evaluation, this study provides a comprehensive structure-to-function framework. Such an approach not only demonstrates the green and efficient synthesis of a Schiff base but also underscores its potential as a lead molecule in drug discovery. Beyond their reported antiviral and anticancer properties, Schiff bases are also well recognised for their antibacterial potential. Considering the increasing threat of multidrug-resistant pathogens such as *Staphylococcus aureus* and *Escherichia coli*, evaluation of antibacterial activity provides essential insight into their therapeutic value. Therefore, in this study, the synthesised Schiff base was also subjected to antibacterial testing against these strains in addition to *in silico* docking studies.

EXPERIMENTAL

Synthesis of Schiff base: The Schiff base was synthesised by condensation of *o*-vanillin (2-hydroxy-3-methoxybenzaldhyde) with 4-chloroaniline in ethanol as solvent. This atom-economical reaction follows the principles of green chemistry, as water is the only byproduct, no catalyst is required and ethanol, a biodegradable solvent, minimizes waste generation. The reaction mixture containing *o*-vanillin (0.01 mol) and 4-chloroaniline (0.01 mol) in ethanol (20 mL) was refluxed for 4 h, during which a red solid precipitated as the condensation proceeded through nucleophilic attack of the amine group on the aldehyde carbonyl carbon followed by water elimination to form the azomethine (–C=N–) bond (**Scheme-I**). The precipitate was filtered, washed with cold ethanol and dried in a desiccator and recrystallisation from ethanol afforded crystalline Schiff base in 80% yield, highlighting the eco-friendly and sustainable nature of the process.

Single crystal X-ray diffraction (SCXRD): A single crystal of the Schiff base was obtained by slow evaporation of its ethanolic solution. The crystal was mounted on a Bruker D8 QUEST FIXED-CHI diffractometer equipped with a PHOTON III CPAD detector and Mo*K*α radiation (λ = 0.71073 Å). Data were collected at room temperature, integrated using SAINT v8.41 and absorption corrections were applied with SADABS. The structure was solved by Intrinsic Phasing (SHELXT) and refined by full-matrix least-squares on F^2 using SHELXL-2019/2. Non-hydrogen atoms were refined anisotropically, while hydrogen atoms were placed in calculated positions and refined using a riding model. Crystallographic data for the Schiff base have been deposited with the Cambridge Crystallographic Data Centre under deposition number CCDC 2480823. Copies of these data are available free of charge from the CCDC at www.ccdc.cam.ac.uk/structures

Molecular docking studies: Docking simulations were performed to explore the binding interactions of the Schiff base with selected protein targets (PDB IDs: 1EVE, 5DEX and 1W6R). The ligand structure was generated from SMILES notation using ChemSketch and converted into a 3D conformation. Protein structures were retrieved from the Protein Data Bank, prepared by removing water molecules and heteroatoms and optimised using BIOVIA Discovery Studio. Docking was carried out with AutoDock Vina and binding affinities are reported in kcal/mol. Visualisation of binding poses identified hydrogen bonding, hydrophobic contacts and π-stacking interactions with active site residues.

ADMET evaluation: Pharmacokinetic properties of the Schiff base were predicted using the SwissADME web server. Parameters such as gastrointestinal absorption, blood–brain barrier permeability, drug-likeness filters, bioavailability score and skin permeation were evaluated to assess its potential as a drug candidate.

Computational toxicity assessment: Toxicity profile of the Schiff base was predicted using the ProTox-II platform. The input structure in SMILES format was analysed for LD_{50} value, organ-specific toxicities, mutagenicity, carcinogenicity and nuclear receptor interactions. This prediction provided early insights into its toxicological risks and overall safety.

Antibacterial activity: The antibacterial activity of the Schiff base was evaluated by the agar well diffusion method. Nutrient agar medium (2.8 μg/100 mL distilled water) was prepared and sterilised by autoclaving at 121 ºC for 15 min. Test organisms (*S. aureus* MTCC 902 and *E. coli* MTCC 443) were cultured in nutrient broth and adjusted to 0.5 OD (McFarland standard). Sterile Petri plates containing 20 mL of nutrient agar were seeded with 24 h cultures. Wells were cut and filled with Schiff base solution at concentrations of 50, 100, 250 and 500 μg/mL. Gentamicin was used as the positive control. After incubation at 37 ºC for 24 h, the antibacterial activity was assessed by measuring the diameter of inhibition zones (mm). Results were expressed as mean ± SD and analysed using GraphPad Prism 6.0 software.

RESULTS AND DISCUSSION

Single crystal X-ray diffraction (SCXRD)

Crystal structure and hydrogen bonding analysis: Single-crystal X-ray diffraction analysis confirmed the structure of

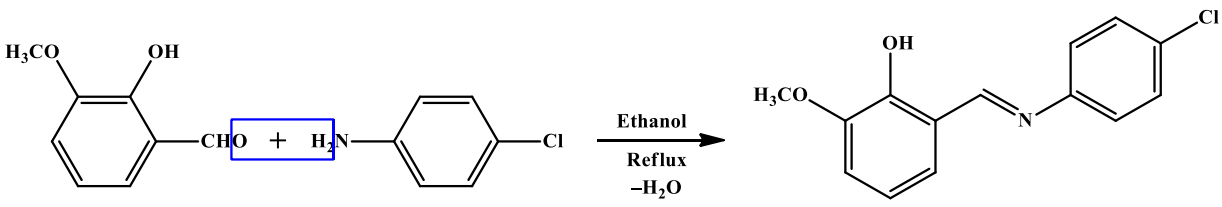

2-Hydroxy-3-methoxy-benzaldehyde (*o*-vanillin) 4-Chloroaniline (*E*)-2-(((4-Chlorophenyl)imino)methyl)-6-methoxyphenol

Scheme-I: Synthesis of Schiff base (*E*)-2-(((4-chlorophenyl)imino)methyl)-6-methoxyphenol

the Schiff base compound, crystallizing in the orthorhombic system with space group $P2_12_12_1$. The detailed crystal data and refinement parameters are summarised in Table-1. The unit cell parameters (a = 4.9058 Å, b = 12.5688 Å, c = 20.1904 Å) correspond to a volume of 1244.94 Å^3 with Z = 4. The refinement converged with a low R value ($R1$ = 0.032) and a goodness-of-fit of 1.03, confirming the reliability of the solved structure [18]. The molecular geometry, depicted in the ORTEP diagram (Fig. 1), reveals a nearly planar arrangement around the azomethine (–CH=N–) linkage [19]. This planarity facilitates extended conjugation between the phenolic and chloroaniline rings, which is characteristic of Schiff bases and enhances both stability and potential biological interactions.

TABLE-1
CRYSTAL DATA AND STRUCTURE REFINEMENT PARAMETERS OF SCHIFF BASE COMPOUND

CCDC number	2480823
Empirical formula	$C_{14}H_{12}ClNO_2$
Formula weight	261.7
Temperature (K)	300(2)
Crystal system	Orthorhombic
Space group (number)	$P2_12_12_1$ (19)
a (Å)	4.9058(4)
b (Å)	12.5688(9)
c (Å)	20.1904(16)
α (°)	90
β (°)	90
γ (°)	90
Volume (Å^3)	1244.94(17)
Z	4
ρ_{calc} (g cm^{-3})	1.396
μ (mm^{-1})	0.299
F(000)	544
Crystal size (mm^3)	0.178×0.209×0.236
Crystal colour	clear light orange
Crystal shape	block
Radiation	Mo$K\alpha$ (λ=0.71073 Å)
2θ range (°)	4.03 to 52.77 (0.80 Å)
Index ranges	–6 ≤ h ≤ 5; –15 ≤ k ≤ 15; –25 ≤ l ≤ 25
Reflections collected	23063
Independent reflections	2531
	R_{int} = 0.0546; R_{sigma} = 0.0273
Completeness to θ = 25.242°	99.6
Data/restraints/parameters	2531/0/166
Goodness-of-fit on F^2	1.027
Final R indexes [$I \geq 2\sigma(I)$]	R_1 = 0.0316
	wR_2 = 0.0830
Final R indexes (all data)	R_1 = 0.0384
	wR_2 = 0.0856
Largest peak/hole (eÅ^{-3})	0.10/–0.19
Flack X parameter	0.04(2)

The packing diagram (Fig. 2) highlights the role of non-covalent interactions in stabilizing the crystal lattice. In particular, hydrogen bonding interactions play a central role in the supramolecular organisation. A strong intramolecular O–H···N hydrogen bond links the hydroxyl substituent with the azomethine nitrogen, reinforcing planarity and conjugation within the molecule. In addition, weak but significant intermolecular contacts such as C–H···O and C–H···Cl interactions extend

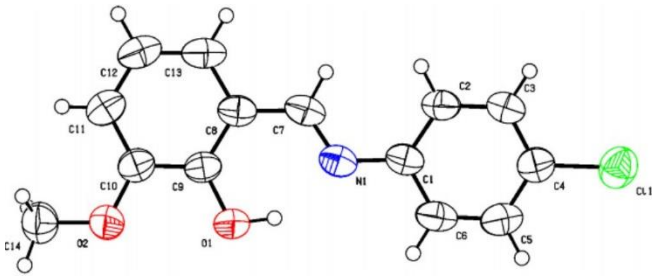

Fig. 1. ORTEP diagram of Schiff base compound with 50% probability ellipsoids

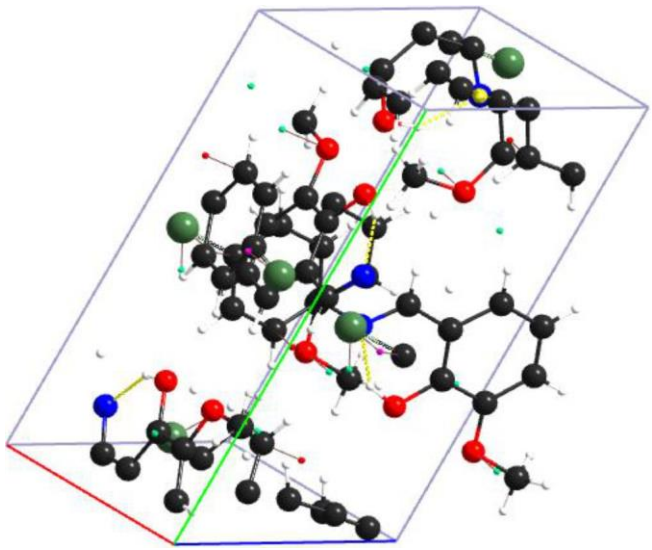

Fig. 2. Crystal packing diagram viewed along the a-axis, showing intermolecular interactions

the crystal packing into a three-dimensional network, as illustrated in Fig. 3.

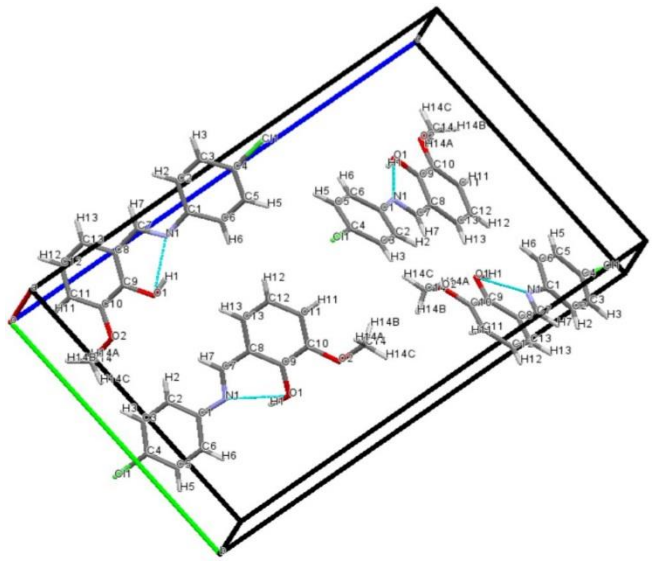

Fig. 3. Hydrogen bonding interactions stabilizing the crystal lattice of Schiff base

The hydrogen bond geometry, presented in Table-2, supports these observations. The O1–H1···N1 intramolecular interaction (D···A = 2.616 Å, ∠DHA = 145°) confirms its role in stabili-

TABLE-2
HYDROGEN BOND GEOMETRY (Å,º) OF SCHIFF BASE LIGAND

D–H···A (Å)	d(D–H) (Å)	d(H···A) (Å)	d(D···A) (Å)	∠(DHA) (º)
C3–H3···O2#1	0.93	2.48	3.338(3)	153.9
C11–H11···Cl1#2	0.93	2.82	3.607(3)	142.9
O1–H1···N1	0.91	1.81	2.616(3)	145.3

Symmetry transformations used to generate equivalent atoms: #1: 1-X, 0.5+Y, 1.5-Z; #2: 0.5-X, 1-Y, 0.5+Z

zing the molecular framework. Meanwhile, the C3–H3···O2 and C11–H11···Cl1 intermolecular contacts (D···A = 3.338 and 3.607 Å, respectively) contribute to the overall supramolecular assembly [20]. Together, these interactions demonstrate that intramolecular hydrogen bonding governs molecular conformation, while intermolecular contacts dictate crystal packing, resulting in a stable and well-ordered lattice.

Binding affinity and interaction profile of Schiff base with selected targets: Molecular docking analysis revealed that the ligand exhibited favourable binding interactions with all three target proteins (1EVE, 1W6R and 5DEX), though the strength and nature of interactions varied (Table-3). For 1EVE, the ligand was well accommodated in the binding pocket, stabilised primarily through a conventional hydrogen bond with Tyr181. Furthermore, π–π stacking interactions with Phe330 and Phe331, along with π–alkyl and van der Waals contacts involving Trp84 and surrounding residues, contributed to the stability of the complex [21]. These multiple non-covalent interactions justify the good binding affinity observed (-8.2 kcal/mol) (Fig. 4a).

In the case of 1W6R, the ligand displayed the strongest binding affinity (-8.4 kcal/mol). This enhanced binding was due to a combination of hydrogen bonding with Ser286 and significant π–π stacking and T-shaped interactions with aromatic residues such as Tyr328, Phe329 and Phe330. Furthermore, hydrophobic contacts with Leu320 and Ile287 helped stabilize the ligand deeper within the active pocket [22]. The abundance of aromatic and hydrophobic interactions explains why this protein showed the most favourable docking score (Fig. 4b). For 5DEX, the binding affinity was comparatively weaker (-7.1 kcal/mol). The ligand established mainly hydrophobic interactions (alkyl and π-alkyl) with Val129, Pro260 and Phe131, along with an electrostatic π-anion interaction with Glu133. However, the absence of strong hydrogen bonding interactions reduced the overall stability of the complex, leading to lower affinity compared to 1EVE and 1W6R (Fig. 4c). Overall, the ligand showed the binding order of 1W6R (-8.4 kcal/mol) > 1EVE (-8.2 kcal/mol) > 5DEX (-7.1 kcal/mol), suggesting that 1W6R is the most favourable target. These proteins were selected for docking since they represent structurally and functionally relevant biomolecular targets in antiviral and antibacterial research, making them suitable for comparative evaluation of ligand affinity and interaction patterns.

Physico-chemical and pharmacokinetic assessment: The physico-chemical and pharmacokinetic properties of the (*E*)-4-chloro-2-[(4-hydroxy-3-methoxybenzylidene)amino]-phenol were predicted using the SwissADME server to evaluate its potential as a drug-like molecule (Table-4). The compound has a molecular weight of 261.70 g/mol, a TPSA of 41.82 Å^2 and three rotatable bonds, all within the favourable ranges for oral bioavailability [23]. The consensus log P value (3.33) indicates moderate lipophilicity, suggesting an appropriate balance between hydrophilic and hydrophobic character. Solubility predictions classified the ligand as soluble to moderately soluble, further supporting its potential for *in vivo* absorption. The BOILED-Egg model predicted high gastrointestinal absorption (HIA) and blood-brain barrier (BBB) permeation [24], with the compound positioned inside the yellow yolk region (Fig. 5). Importantly, the ligand was not identified as a P-glycoprotein substrate, suggesting reduced efflux probability and improved systemic retention.

The bioavailability radar revealed that the ligand falls within the optimal range for lipophilicity, size, polarity, solubility and flexibility, whereas only the saturation parameter (INSATU) deviates slightly due to a low fraction of sp^3 carbons (Fig. 5). Such deviations are typical for planar aromatic Schiff bases and generally do not hinder drug-likeness. Evaluation against standard drug-likeness filters (Lipinski, Ghose, Veber, Egan, Muegge) confirmed no violations [25]. The compound was free from PAINS alerts and displayed only one Brenk alert (imine

TABLE-3
DOCKING RESULTS OF SCHIFF BASE LIGAND WITH TARGET PROTEINS (1EVE, 1W6R, 5DEX) SHOWING BINDING AFFINITIES (kcal/mol) AND RMSD VALUES

Mode	Affinity (kcal/mol)			RMSD l.b.			RMSD u.b.		
	1EVE	1W6R	5DEX	1EVE	1W6R	5DEX	1EVE	1W6R	5DEX
1	-8.2	-8.4	-7.1	0.000	0.000	0.000	0.000	0.000	0.000
2	-8.2	-8.3	-7.0	2.520	4.626	20.855	2.946	8.571	21.866
3	-8.1	-8.3	-6.8	3.888	4.513	18.220	7.304	8.748	19.628
4	-8.0	-8.2	-6.7	4.266	2.553	10.231	8.065	3.569	11.709
5	-7.9	-8.2	-6.7	2.370	3.105	3.799	3.319	4.569	7.360
6	-7.8	-7.9	-6.7	2.085	4.792	20.878	2.697	9.072	21.982
7	-7.8	-7.7	-6.7	3.054	2.407	9.708	3.676	3.473	11.099
8	-7.7	-7.7	-6.6	3.693	4.675	11.039	7.182	8.353	11.624
9	-7.5	-7.6	-6.6	4.147	2.784	9.648	7.536	4.309	10.555

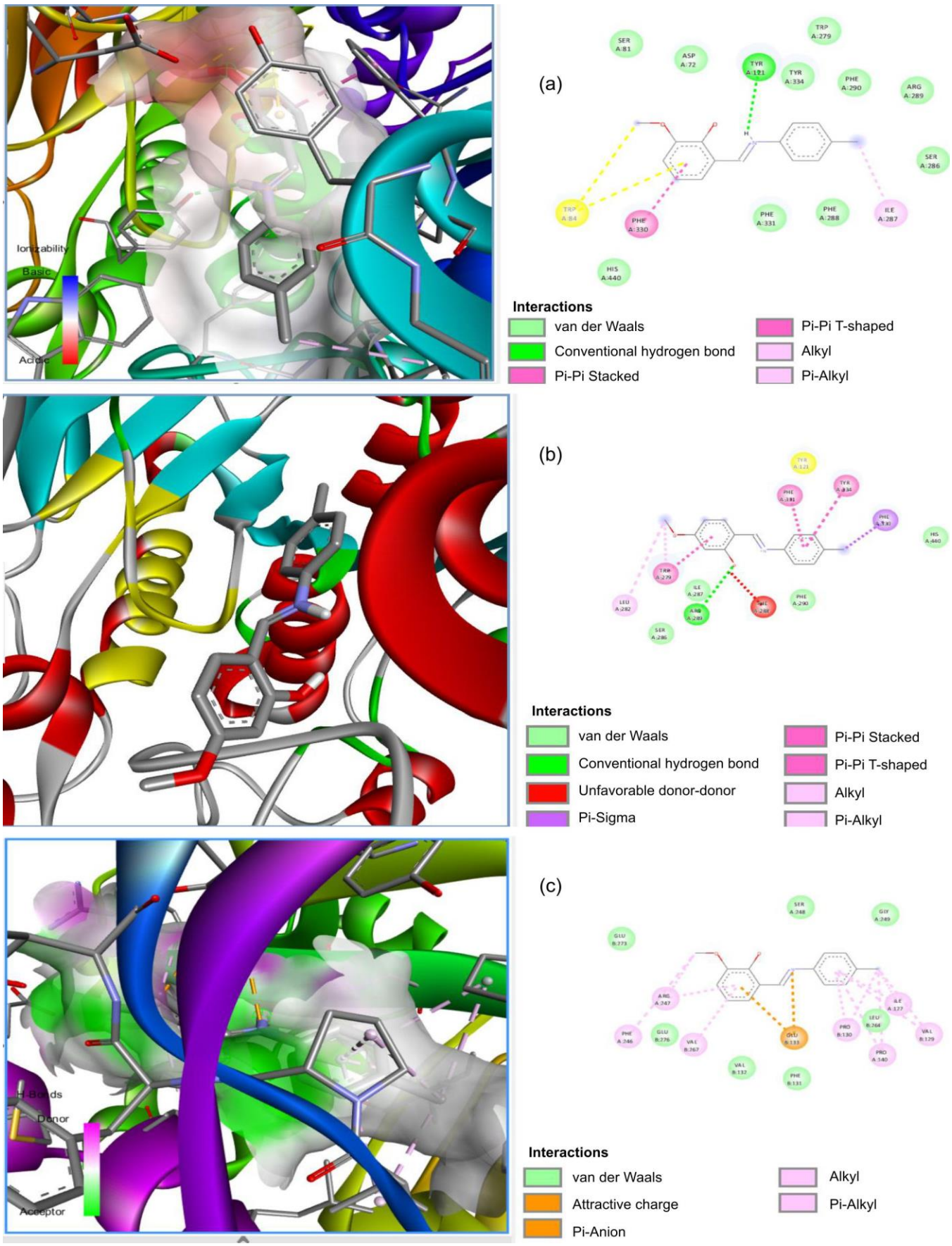

Fig. 4. 3D and 2D interaction diagrams of the Schiff base ligand with target proteins: (a) 1EVE, (b) 1W6R and (c) 5DEX

TABLE-4
SwissADME-PREDICTED PHYSICO-CHEMICAL, PHARMACOKINETIC AND DRUG-LIKENESS PROPERTIES OF SCHIFF BASE LIGAND

SMILES	COc1ccc(c(c1)O)C=Nc1ccc(cc1)Cl
Physico-chemical properties	
Formula	$C_{14}H_{12}ClNO_2$
Molecular weight	261.70 g/mol
Num. heavy atoms	18
Num. arom. heavy atoms	12
Fraction Csp^3	0.07
Num. rotatable bonds	3
Num. H-bond acceptors	3
Num. H-bond donors	1
Molar refractivity	73.66
TPSA	41.82 Å^2
Lipophilicity	
Log $P_{o/w}$ (iLOGP)	2.59
Log $P_{o/w}$ (XLOGP3)	3.47
Log $P_{o/w}$ (WLOGP)	3.80
Log $P_{o/w}$ (MLOGP)	2.78
Log $P_{o/w}$ (SILICOS-IT)	4.01
Consensus Log $P_{o/w}$	3.33
Water solubility	
Log S (ESOL)	-3.94
Solubility	2.98×10^{-2} mg/mL; 1.14×10^{-4} mol/L
Class	Soluble
Log S (Ali)	-4.03
Solubility	2.44×10^{-2} mg/mL; 9.33×10^{-5} mol/L
Class	Moderately soluble
Log S (SILICOS-IT)	-5.18
Solubility	1.73×10^{-3} mg/mL; 6.62×10^{-6} mol/L
Class	Moderately soluble
Pharmacokinetics	
GI absorption	High
BBB permeant	Yes
P-gp substrate	No
CYP1A2 inhibitor	Yes
CYP2C19 inhibitor	Yes
CYP2C9 inhibitor	Yes
CYP2D6 inhibitor	No
CYP3A4 inhibitor	Yes
Log K_p (skin permeation)	-5.43 cm/s
Druglikeness	
Lipinski	Yes; 0 violation
Ghose	Yes
Veber	Yes
Egan	Yes
Muegge	Yes
Bioavailability score	0.55
Medicinal chemistry	
PAINS	0 alert
Brenk	1 alert: imine_1
Leadlikeness	Yes
Synthetic accessibility	2.37

group). A bioavailability score of 0.55 indicates moderate oral availability and the synthetic accessibility score (2.37) suggests that the ligand can be synthesised with relative ease. Overall, the ADMET profile demonstrates that the Schiff base ligand possesses a favourable physico-chemical balance, oral bioavailability and pharmacokinetic properties, making it a promising candidate for further development in anticancer studies.

Computational toxicity assessment: The ProTox-II predictions for (*E*)-4-chloro-2-[(4-hydroxy-3-methoxybenzylidene)-amino]phenol indicated a mixed safety profile (Table-5 and Fig. 6). Hepatotoxicity (0.52), neurotoxicity (0.69) and immunotoxicity (0.69) were flagged as potential risks, while respiratory toxicity, nephrotoxicity, cardiotoxicity and cytotoxicity were predicted as inactive [26]. Moderate probabilities were observed for carcinogenicity (0.51), mutagenicity (0.50) and clinical toxicity (0.52). Blood-brain barrier penetration was strongly predicted (0.78), consistent with SwissADME results.

Mitochondrial membrane potential disruption (0.70) emerged as the key stress response, whereas nuclear receptor interactions were minimal, except for aryl hydrocarbon receptor activity (0.61). Strong binding to transthyretin (0.84) suggested possible endocrine or transport-related implications [27]. Metabolic profiling indicated involvement of CYP1A2, CYP2C19, CYP2C9 and CYP2D6, but not CYP3A4 or CYP2E1. Collectively, these results highlight favourable ADME properties alongside toxicity liabilities that require further experimental validation [28].

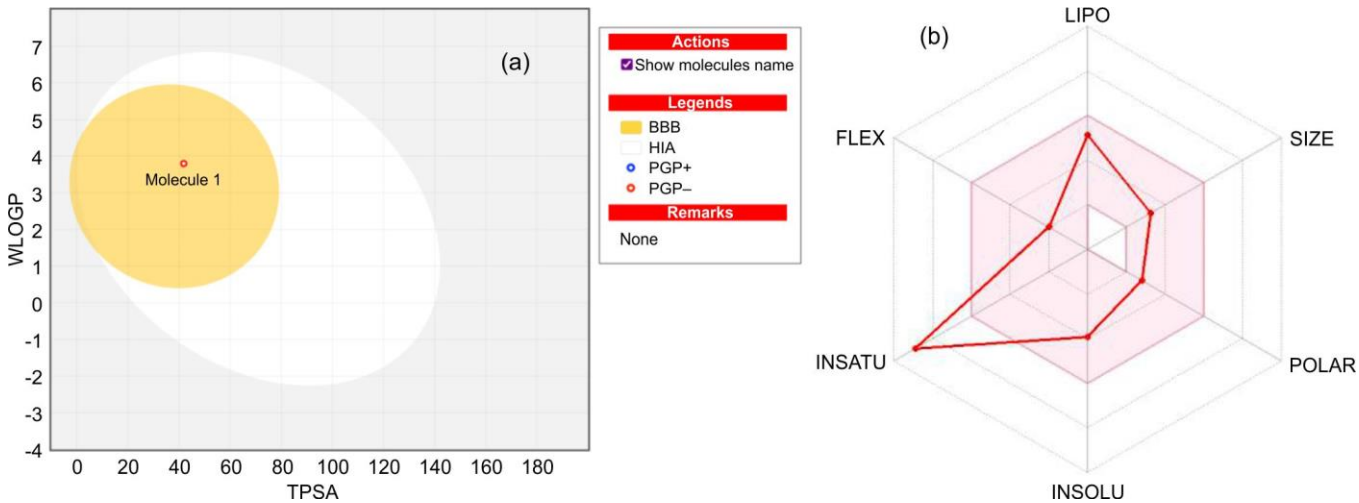

Fig. 5. SwissADME BOILED-Egg (a) showing high GI absorption and BBB permeation and bioavailability radar (b) displaying drug-likeness profile of Schiff base compound

TABLE-5
ProTox-II PREDICTED TOXICITY AND METABOLIC PROFILE OF SCHIFF BASE COMPOUND

Classification	Target	Shorthand	Prediction	Probability
Organ toxicity	Hepatotoxicity	dili	Active	0.52
Organ toxicity	Neurotoxicity	neuro	Active	0.69
Organ toxicity	Nephrotoxicity	nephro	Inactive	0.52
Organ toxicity	Respiratory toxicity	respi	Inactive	0.56
Organ toxicity	Cardiotoxicity	cardio	Inactive	0.66
Toxicity end points	Carcinogenicity	carcino	Active	0.51
Toxicity end points	Immunotoxicity	immuno	Active	0.69
Toxicity end points	Mutagenicity	mutagen	Active	0.50
Toxicity end points	Cytotoxicity	cyto	Inactive	0.60
Toxicity end points	BBB-barrier	bbb	Active	0.78
Toxicity end points	Ecotoxicity	eco	Active	0.64
Toxicity end points	Clinical toxicity	clinical	Active	0.52
Toxicity end points	Nutritional toxicity	nutri	Inactive	0.73
Tox21-Nuclear receptor signalling pathways	Aryl hydrocarbon receptor (AhR)	nr_ahr	Active	0.61
Tox21-Nuclear receptor signalling pathways	Androgen receptor (AR)	nr_ar	Inactive	0.97
Tox21-Nuclear receptor signalling pathways	Androgen receptor ligand binding domain (AR-LBD)	nr_ar_lbd	Inactive	0.99
Tox21-Nuclear receptor signalling pathways	Aromatase	nr_aromatase	Inactive	0.64
Tox21-Nuclear receptor signalling pathways	Estrogen receptor alpha (ER)	nr_er	Inactive	0.67
Tox21-Nuclear receptor signalling pathways	Estrogen receptor ligand binding domain (ER-LBD)	nr_er_lbd	Inactive	0.85
Tox21-Nuclear receptor signalling pathways	Peroxisome proliferator activated receptor gamma (PPAR-Gamma)	nr_ppar_gamma	Inactive	0.84
Tox21-Stress response pathways	Nuclear factor (erythroid-derived 2)-like 2/antioxidant responsive element (nrf2/ARE)	sr_are	Inactive	0.74
Tox21-Stress response pathways	Heat shock factor response element (HSE)	sr_hse	Inactive	0.74
Tox21-Stress response pathways	Mitochondrial membrane potential (MMP)	sr_mmp	Active	0.70
Tox21-Stress response pathways	Phosphoprotein (tumor supressor) p53	sr_p53	Inactive	0.78
Tox21-Stress response pathways	ATPase family AAA domain-containing protein 5 (ATAD5)	sr_atad5	Inactive	0.80
Molecular initiating events	Thyroid hormone receptor alpha (THRα)	mie_thr_alpha	Inactive	0.81
Molecular initiating events	Thyroid hormone receptor beta (THRβ)	mie_thr_beta	Inactive	0.86
Molecular initiating events	Transtyretrin (TTR)	mie_ttr	Active	0.84
Molecular initiating events	Ryanodine receptor (RYR)	mie_ryr	Inactive	0.95
Molecular initiating events	GABA receptor (GABAR)	mie_gabar	Inactive	0.71
Molecular initiating events	Glutamate N-methyl-D-aspartate receptor (NMDAR)	mie_nmdar	Inactive	0.90
Molecular initiating events	α-Amino-3-hydroxy-5-methyl-4-isoxazolepropionate receptor (AMPAR)	mie_ampar	Inactive	1.0
Molecular initiating events	Kainate receptor (KAR)	mie_kar	Inactive	1.0
Molecular initiating events	Achetylcholinesterase (AChE)	mie_ache	Inactive	0.92
Molecular initiating events	Constitutive androstane receptor (CAR)	mie_car	Inactive	0.99
Molecular initiating events	Pregnane X receptor (PXR)	mie_pxr	Inactive	0.82
Molecular initiating events	NADH-quinone oxidoreductase (NADHOX)	mie_nadhox	Inactive	0.90
Molecular initiating events	Voltage gated sodium channel (VGSC)	mie_vgsc	Inactive	0.79
Molecular initiating events	Na^+/I^- symporter (NIS)	mie_nis	Inactive	0.99
Metabolism	Cytochrome CYP1A2	CYP1A2	Active	0.71
Metabolism	Cytochrome CYP2C19	CYP2C19	Active	0.58
Metabolism	Cytochrome CYP2C9	CYP2C9	Active	0.66
Metabolism	Cytochrome CYP2D6	CYP2D6	Active	0.51
Metabolism	Cytochrome CYP3A4	CYP3A4	Inactive	0.77
Metabolism	Cytochrome CYP2E1	CYP2E1	Inactive	1.0

Antibacterial evaluation: Inspired by molecular docking results showing favourable binding of 4CAOV with bacterial DNA gyrase (PDB ID: 5DEX), compound was experimentally evaluated for its antibacterial efficacy [29]. The synthesised Schiff base exhibited potent, concentration-dependent antibacterial activity against both *S. aureus* (Gram-positive) and *E. coli* (Gram-negative). At 500 μg/mL (Fig. 7a-b), 4CAOV exhibited inhibition zones of 21.10 ± 0.56 mm for *S. aureus* and 21.60 ± 0.56 mm for *E. coli*, both values exceeding those of the standard drug gentamicin (15.35 ± 0.49 mm and 15.60 ± 0.56 mm, respectively). Even at the lowest concentration (50 μg/mL), notable inhibition was observed, with *E. coli* (13.35 ± 0.21 mm) showing slightly greater sensitivity than *S. aureus* (11.35 ± 0.21 mm).

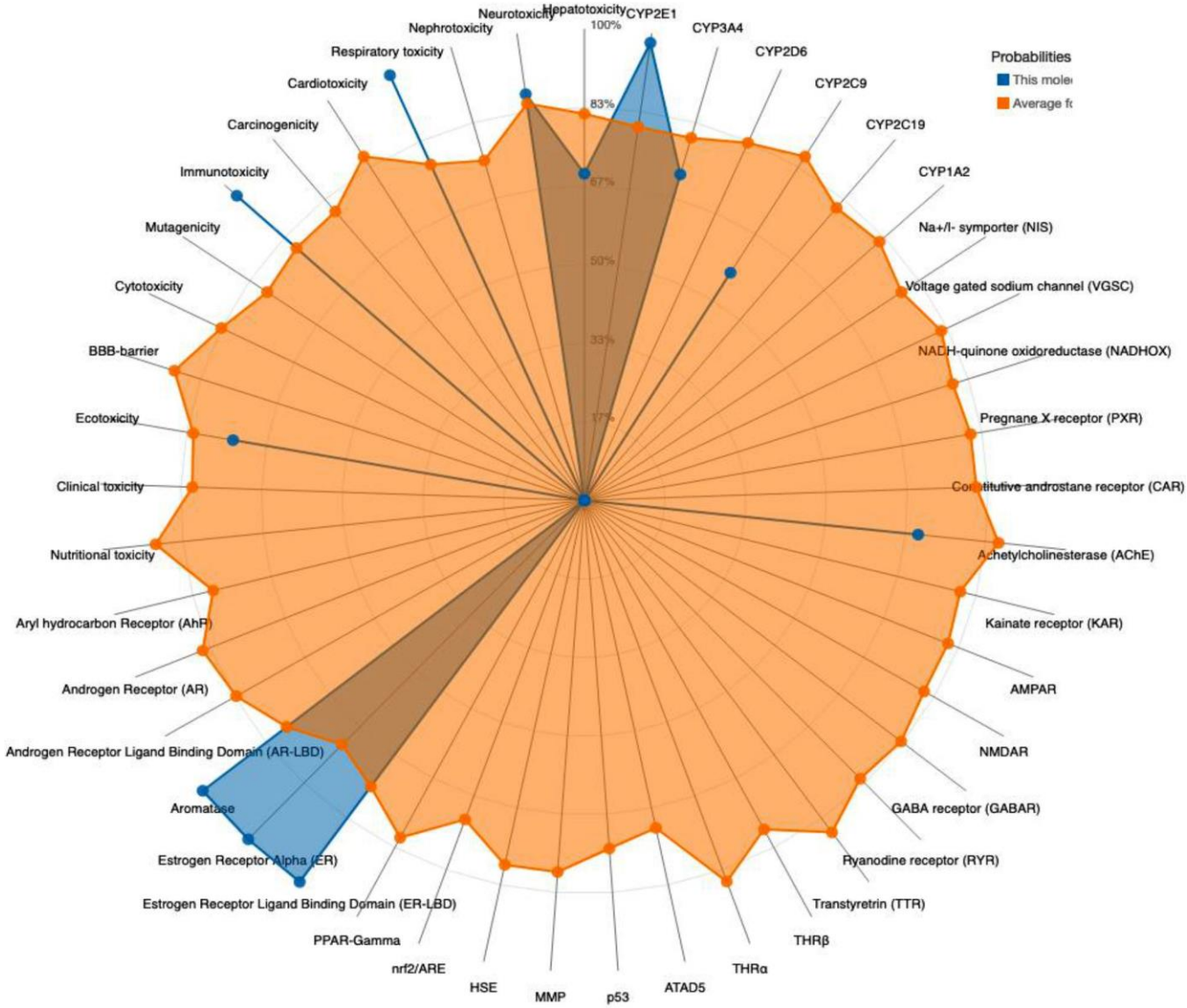

Fig. 6. ProTox-II radar plot of predicted toxicity endpoints and molecular initiating events for Schiff base compound

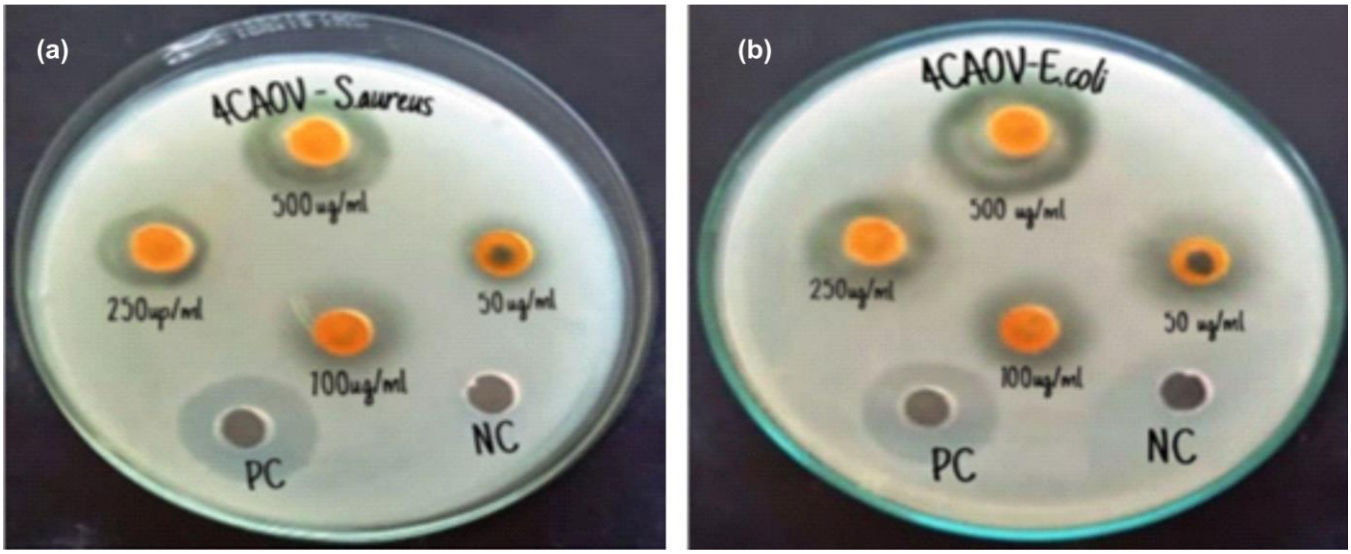

Fig. 7. Antibacterial activity of the Schiff base (4CAOV) against (a) *S. aureus* and (b) *E. coli* by agar well diffusion method

The results of these experiments suggest that 4CAOV is an antibacterial compound which is effective against both Gram-positive and Gram-negative bacteria, with slightly higher potential effect on *E. coli*. The reason for the increased response by the Gram-negative bacteria may be due to an increased ability of this compound to penetrate through their thinner peptidoglycan layers, and a better affinity for the enzymes in the membrane that can interact with this compound. The strong antibacterial activity of 4CAOV may be attributed to the azomethine (-C=N-) bond in its structure as well as the numerous phenolic groups which may facilitate the interaction between 4CAOV and the proteins and enzymes of these different types of bacteria. Thus, 4CAOV showed superior antibacterial activity over gentamicin against both strains.

Conclusion

In this study, a novel Schiff base was synthesised through a green, catalyst-free approach and structurally confirmed by single-crystal X-ray diffraction, with a lattice stabilised by intramolecular hydrogen bonding and intermolecular interactions. Molecular docking studies indicated strong binding affinity toward bacterial DNA gyrase B, which was reflected in its potent antibacterial activity against both Gram-positive (*S. aureus*) and Gram-negative (*E. coli*) strains. The compound exhibited concentration-dependent inhibition, surpassing the standard drug gentamicin at higher concentrations, with *E. coli* showing slightly greater sensitivity. The favourable physicochemical, pharmacokinetic and toxicity profiles further support its drug-likeness and safety. Thus, these findings highlight the Schiff base as a structurally robust and highly effective antibacterial agent, presenting a promising scaffold for the development of new antibacterial therapeutics.

ACKNOWLEDGEMENTS

The authors sincerely acknowledge the Managing Trustee and the Director of Academics, Seethalakshmi Ramaswami College (Affiliated to Bharathidasan University), for granting access to the institutional facilities necessary for carrying out this work.

CONFLICT OF INTEREST

The authors declare that there is no conflict of interests regarding the publication of this article.

DECLARATION OF AI-ASSISTED TECHNOLOGIES

The authors declare that no AI tools were used in the preparation or writing of this research/review article.

REFERENCES

1. Q. Guan, S. Xing, L. Wang, J. Zhu, C. Guo, C. Xu, Q. Zhao, Y. Wu, Y. Chen and H. Sun, *J. Med. Chem.*, **67**, 7788 (2024); https://doi.org/10.1021/acs.jmedchem.4c00652
2. P. Taylor, R.P. Robinson, Y.M. Fobian, D.C. Blakemore, L.H. Jones and O. Fadeyi, *Org. Biomol. Chem.*, **14**, 6611 (2016); https://doi.org/10.1039/C6OB00936K
3. O.O. Grygorenko, D.M. Volochnyuk, S.V. Ryabukhin and D.B. Judd, *Chemistry*, **26**, 1196 (2020); https://doi.org/10.1002/chem.201903232
4. C. Castiello, P. Junghanns, A. Mergel, C. Jacob, C. Ducho, S. Valente, D. Rotili, R. Fioravanti, C. Zwergel and A. Mai, *Green Chem.*, **25**, 2109 (2023); https://doi.org/10.1039/D2GC03772F
5. V. Govindaraj, P. Mathiazhagan G, S. Ramanathan, K. Elavalagan and R. Renganathan, *Bull. Chem. Soc. Ethiop.*, **39**, 1071 (2025); https://doi.org/10.4314/bcse.v39i6.4
6. T. Nasiriani, S. Javanbakht, M.T. Nazeri, H. Farhid, V. Khodkari and A. Shaabani, *Top. Curr. Chem.*, **380**, 50 (2022); https://doi.org/10.1007/s41061-022-00403-8
7. G.-W. Wang, *Chem. Soc. Rev.*, **42**, 7668 (2013); https://doi.org/10.1039/c3cs35526h
8. P. Ghamari Kargar, S. Aryanejad and G. Bagherzade, *Appl. Organomet. Chem.*, **34**, e5965 (2020); https://doi.org/10.1002/aoc.5965
9. G. Valarmathy, R. Subbalakshmi, R. Sumathi and R. Renganathan, *J. Mol. Struct.*, **1199**, 127029 (2020); https://doi.org/10.1016/j.molstruc.2019.127029
10. M.A. Mir and B.K. Banik, *Inorg. Chem. Commun.*, **174**, 113987 (2025); https://doi.org/10.1016/j.inoche.2025.113987
11. I. Waziri, S. Sookai, T.L. Yusuf, K.A. Olofinsan and A.J. Muller, *Appl. Organomet. Chem.*, **39**, e70162 (2025); https://doi.org/10.1002/aoc.70162
12. E. Uddin, M.N. Sardar, M.S. Reza, M.S. Hasan, M.T. Talukder, M.M. Hoque, P. Paul, M.S. Khatun, M.F. Hossen, M.A. Asraf and M. Kudrat-E-Zahan, *Discov. Chem.*, **2**, 153 (2025); https://doi.org/10.1007/s44371-025-00228-6
13. A.M. Asran, A.K. Aldhalmi, E.N.A. Musa, A.A. Fayek, M.S.A. Mansour and A.A. El-Sherif, *Inorg. Chem. Commun.*, **171**, 113371 (2025); https://doi.org/10.1016/j.inoche.2024.113371
14. P.M. Thakor, R.J. Patel, R.K. Giri, S.H. Chaki, A.J. Khimani, Y.H. Vaidya, P. Thakor, A.B. Thakkar and J.D. Patel, *ACS Omega*, **8**, 33069 (2023); https://doi.org/10.1021/acsomega.3c05254
15. U. Naithani and V. Guleria, *Front. Drug Discov.*, **4**, 1362456 (2024); https://doi.org/10.3389/fddsv.2024.1362456
16. K.M. Krupka, M. Pochec, J.J. Panek and A. Jezierska, *Int. J. Mol. Sci.*, **23**, 12439 (2022); https://doi.org/10.3390/ijms232012439
17. C.P. Constantinides, S. Raza, F. Bazzi, N. Sharara and S. Marincean, *Crystals*, **15**, 732 (2025); https://doi.org/10.3390/cryst15080732
18. N. Archana, M. Vijayasri, K. Dayanidhi and S. Parthiban, *Transition Met. Chem.*, **50**, 949 (2025); https://doi.org/10.1007/s11243-025-00669-z
19. G.M. Sheldrick, *Acta Crystallogr. A Found. Adv.*, **71**, 3 (2015); https://doi.org/10.1107/S2053273314026370
20. A. Šagátová, I. Nemec, J. Moncoľ, R. Herchel, R. Šebesta, P. Kisszékelyi, L. Ďurina and I. Šalitroš, *Inorg. Chem. Front.*, **12**, 8173 (2025); https://doi.org/10.1039/D5QI01269D
21. L.G. Khatik, *Int. J. Green Pharm.*, **12**, 1824 (2018); https://doi.org/10.22377/ijgp.v12i02.1824
22. M.D. Gambardella, Y. Wang and J. Pang, *Molecules*, **29**, 2333 (2024); https://doi.org/10.3390/molecules29102333
23. S. Ramasamy and A.T. Rajan, *J. Fluoresc.*, **32**, 1873 (2022); https://doi.org/10.1007/s10895-022-02987-2
24. L.A. Vélez, Y. Delgado, Y. Ferrer-Acosta, I.J. Suárez-Arroyo, P. Rodríguez and D. Pérez, *Int. J. Plant Biol.*, **13**, 163 (2022); https://doi.org/10.3390/ijpb13020016
25. A. Haruna, I.T. Sirajo, M.M. Rumah and Y. Albashir, *J. Res. Appl. Sci. Biotechnol.*, **2**, 58 (2023); https://doi.org/10.55544/jrasb.2.6.10
26. J. Hakkola, J. Hukkanen, M. Turpeinen and O. Pelkonen, *Arch. Toxicol.*, **94**, 3671 (2020); https://doi.org/10.1007/s00204-020-02936-7
27. S.S. Alghamdi, R.S. Suliman, N.A. Aljammaz, K.M. Kahtani, D.A. Aljatli and G.M. Albadrani, *Plants*, **11**, 549 (2022); https://doi.org/10.3390/plants11040549
28. Y.S. Kiani and I. Jabeen, *ACS Omega*, **5**, 179 (2019); https://doi.org/10.1021/acsomega.9b02344
29. E. Kenawy, S. Khattab and M.M. Azaam, *Delta J. Sci.*, **40**, 69 (2019); https://doi.org/10.21608/djs.2019.139205